Fluorescent Imaging of Single Nanoparticles and Viruses on a Smart Phone

Qingshan Wei,[†,‡,§] Hangfei Qi,[∥] Wei Luo,[†] Derek Tseng,[†] So Jung Ki,[⊥] Zhe Wan,[†] Zoltán Göröcs,[†,‡] Laurent A. Bentolila,[§,⊥] Ting-Ting Wu,[∥] Ren Sun,[§,∥] and Aydogan Ozcan[†,‡,§,*]

[†]Electrical Engineering Department, [‡]Bioengineering Department, [§]California NanoSystems Institute (CNSI), [∥]Department of Molecular and Medical Pharmacology, and [⊥]Department of Chemistry and Biochemistry, University of California, Los Angeles (UCLA), California 90095, United States

ABSTRACT Optical imaging of nanoscale objects, whether it is based on scattering or fluorescence, is a challenging task due to reduced detection signal-to-noise ratio and contrast at subwavelength dimensions. Here, we report a field-portable fluorescence microscopy platform installed on a smart phone for imaging of individual nanoparticles as well as viruses using a lightweight and compact opto-mechanical attachment to the existing camera module of the cell phone. This hand-held fluorescent imaging device utilizes (i) a compact 450 nm laser diode that creates oblique excitation on the sample plane with an incidence angle of ~75°, (ii) a long-pass thin-film interference filter to reject the scattered excitation light, (iii) an external lens creating 2× optical magnification, and (iv) a translation stage for focus adjustment. We tested the imaging performance of this smart-phone-enabled microscopy platform by detecting isolated 100 nm fluorescent particles as well as individual human cytomegaloviruses that are fluorescently labeled. The size of each detected nano-object on the cell phone platform was validated using scanning electron microscopy images of the same samples. This field-portable fluorescence microscopy attachment to the cell phone, weighing only ~186 g, could be used for specific and sensitive imaging of subwavelength objects including various bacteria and viruses and, therefore, could provide a valuable platform for the practice of nanotechnology in field settings and for conducting viral load measurements and other biomedical tests even in remote and resource-limited environments.

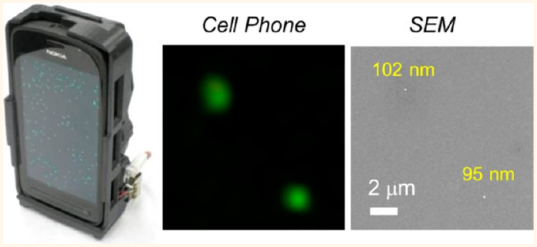

KEYWORDS: cell phone microscopy · fluorescence imaging · single nanoparticle · single virus imaging

Optical imaging of single nanoparticles has become increasingly important for various fields such as nanoscience and biomedicine.[1,2] With the recent advances in light microscopy techniques, individual nanoparticles as small as a few nanometers have been visualized by a number of imaging methods, such as photothermal imaging,[3] interferometric[4,5] and dark-field scattering microscopy,[6,7] among others.[8,9] However, conventional imaging methods used for the detection of isolated subwavelength particles all rely on relatively sophisticated and expensive microscopy systems, which also involve high numerical aperture (NA) objective lenses and other bulky optical components, with a small imaging field-of-view (FOV) of <0.2 mm^2. We have recently demonstrated a lens-free holographic imaging technique which can detect sub-100 nm particles across a large FOV of >20 mm^2; on the other hand, this approach relies on bright-field coherent imaging and is *not* applicable to a fluorescent specimen due to the lack of sufficient spatial and temporal coherence.[9]

Here we demonstrate a compact and lightweight opto-mechanical attachment to the existing camera module of a smart phone for detection of individual fluorescent nanoparticles and viruses. This field-portable fluorescent imager on the cell phone involves a compact laser-diode-based excitation at 450 nm that illuminates the sample plane at a high incidence angle, a long-pass (LP) thin-film interference filter, an external low NA lens, and a coarse mechanical translation stage for focusing and depth adjustment (see Figure 1). The oblique illumination light on the sample plane is by and large missed by the low NA of the external collection lens, and only the scattered excitation beam needs to

* Address correspondence to ozcan@ucla.edu.

Received for review July 22, 2013 and accepted September 9, 2013.

Published online September 09, 2013
10.1021/nn4037706

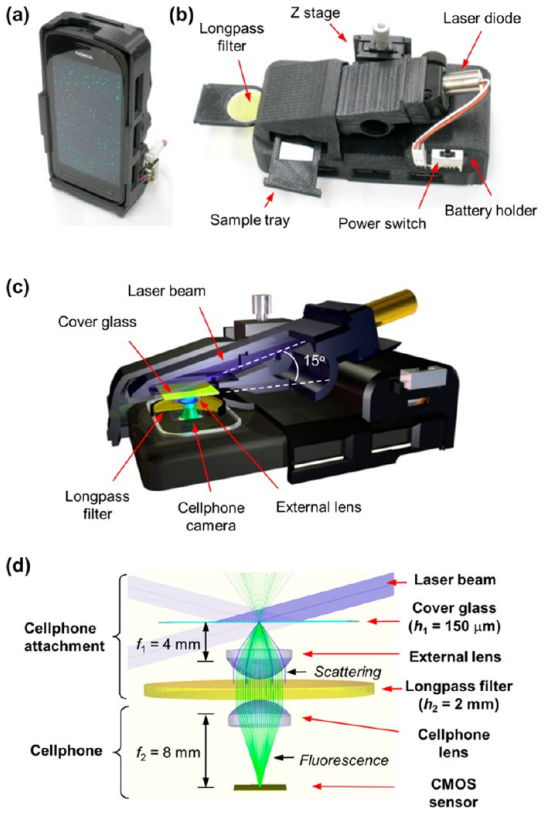

Figure 1. (a–d) Photographs and schematics of our cell-phone-based fluorescence microscope. The screen of the cell phone in (a) shows the fluorescence image of 1 μm diameter green fluorescent beads. A back view of the same cell phone attachment is shown in (b), and its schematic illustration is provided in (c). Ray-tracing diagram of the cell phone microscope is shown in (d), where excitation and scattered beams are indicated with solid blue rays, while the fluorescent emission is highlighted with solid green rays.

be blocked through the LP filter, creating a very efficient background rejection mechanism that is necessary to isolate the extremely weak fluorescent signal arising from individual nanoparticles or viruses. The same low NA imaging system is also useful for reducing the alignment sensitivity to depth of field, such that a coarse mechanical translation stage would be sufficient to focus the cell phone microscope to the sample plane even in field conditions.

We tested the imaging performance of this smartphone-based fluorescent microscopy platform using 100 nm fluorescent particles as well as labeled human cytomegaloviruses (HCMV)—a virus type that is known to cause significant morbidity and mortality in immunocompromised patients.[10] To make sure that indeed single nanoparticles or viruses are detected, each sample was also imaged by scanning electron microscopy (SEM) to validate our cell-phone-based imaging results. These results constitute the first time that a cell-phone-based field-portable imaging platform has been able to detect single viruses or deeply subwavelength objects. We believe that the new imaging performance reached through this work would provide a complementary addition to various other cell-phone-based microscopy, sensing, and diagnostics tools,[11−26] which might provide new opportunities for the practice of nanotechnology in telemedicine and point-of-care (POC) applications, among others.

RESULTS AND DISCUSSION

Hand-Held Fluorescence Microscopy on a Cell Phone. We created a field-portable, mechanically robust, and functional opto-mechanical attachment to the existing camera module of a smart phone that integrates multiple components such as the excitation light source, power unit, sample holder, focusing stage, and imaging optics including, for example, an external lens (focal distance, f_1 = 4 mm) and a thin-film interference-based LP filter (Figure 1a,b).

Some of the major challenges for field-portable imaging of individual nanoscale fluorescent particles/objects on a cell phone microscopy platform are related to the weak fluorescent signal arising from such small-scale objects in addition to the noise background created by the excitation light leakage and detection noise. To overcome some of these signal-to-noise ratio (SNR)-related limitations, a high-power compact laser diode (75 mW) was installed as the excitation source to illuminate the sample plane with a rather high incidence angle of ~75° (Figure 1c). This oblique illumination angle is very important to reduce the background noise in our fluorescent cell phone images as also illustrated in the ray-tracing simulation of our cell phone fluorescence microscope (see Figure 1d). The directly transmitted excitation light (dashed blue rays, Figure 1d) is missed by the low NA detection optics, except for the scattered photons that are mapped onto the cell phone sensor array (solid blue rays). To further clean the background noise and get rid of such scattered excitation photons, we also employed a thin-film-based LP filter with a blocking wavelength of 500 nm and a sharp transmission slope which strongly attenuates shorter wavelengths, such as the scattered excitation light (Supporting Information Figure S1a). This combination of high-angle excitation illumination and high-performance LP filter enabled us to achieve a very high contrast on the cell phone microscope that is required for imaging of isolated fluorescent nanoparticles and viruses (Figure 1d).

During our imaging experiments, air-dried samples (fluorescent particles or fixed viruses) were supported by a cover glass (18 × 18 mm, 150 μm thickness) and were held by a movable sample tray that is inserted to the cell phone opto-mechanical attachment from the side (Figure 1b). Liquid samples can also be imaged on the same cell phone microscopy platform using disposable microfluidic devices or simply between two cover glasses that are sealed. The sample chamber and the laser source are integrated on an adjustable platform which is coupled to a miniature dovetail stage

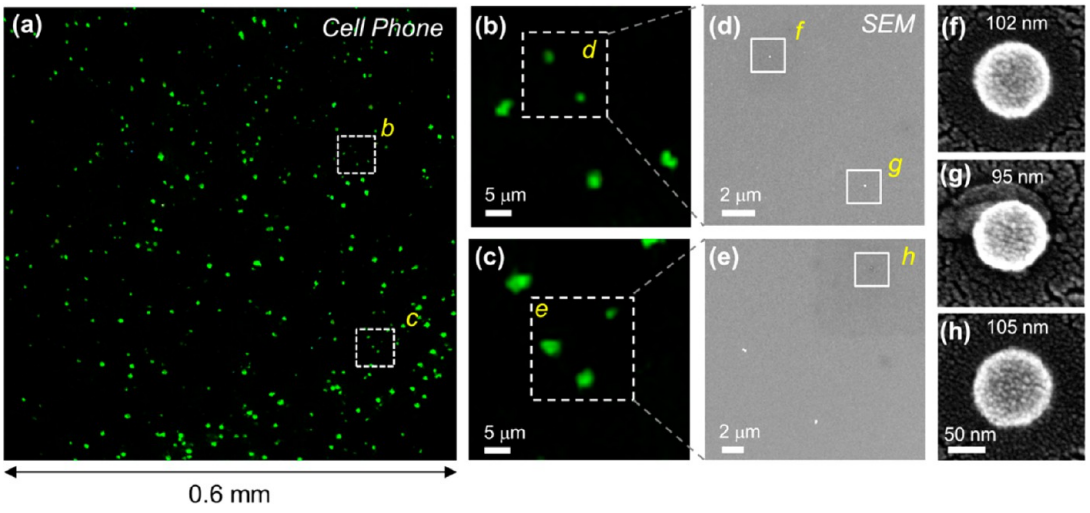

Figure 2. Imaging of 100 nm fluorescent particles on the cell phone. (a) Cell phone fluorescence image of 100 nm PS nanoparticles detected over an area of 0.6 mm × 0.6 mm. (b,c) Enlarged ROIs from the dashed squares in (a). (d,e) SEM images that correspond to the dashed boxes in (b) and (c), respectively. (f–h) High-magnification SEM images of individual fluorescent nanoparticles as indicated by the solid boxes in (d) and (e).

for focus adjustment along the *z* direction. This optomechanical attachment also serves as a light shield unit which protects the users from exposure to our excitation laser (75 mW) and permits highly sensitive fluorescence imaging experiments to be conducted even in the presence of strong ambient light.

Single-Nanoparticle Imaging Experiments. The performance of our cell phone fluorescence microscope was first tested by imaging fluorescent polystyrene (PS) beads with different sizes (ranging from 10 μm down to 100 nm; see Figure S2). Figure 2a shows a typical fluorescence image of 100 nm fluorescent particles obtained by our cell phone microscope with an exposure time of 0.5 s. Two representative regions of interests (ROIs) are also highlighted by dashed white boxes and enlarged in Figure 2b,c, respectively. The brighter and bigger spots in these images are attributed to the clustering of nanoparticles (see, for example, Figure 3), whereas single 100 nm particles appear to be weaker and smaller, as shown in the dashed boxes in Figure 2b,c. The detection of isolated 100 nm particles on our cell phone microscope was independently validated by imaging the same regions of our samples with SEM: Figure 2d,e illustrates SEM images that correspond to the same ROIs within the dashed boxes in Figure 2b,c, respectively. Three individual nanoparticles are shown in solid boxes (Figure 2d,e), and higher-magnification SEM images indicate that the sizes of these particles are 102, 95, and 105 nm, respectively (Figure 2f–h).

We further validated that the detected signals on our cell phone images were indeed due to fluorescence (but not due to scattering of excitation light) by mixing nonfluorescent PS particles with fluorescent samples of comparable sizes and imaging the mixture of these particles both with (w/) and without (w/o) the LP emission filter. Specifically, 1 μm fluorescent particles were mixed with 1 μm nonfluorescent ones, and 500, 250, and 100 nm fluorescent particles were mixed with 500 nm nonfluorescent particles. The color of the fluorescent nanoparticles imaged on our cell phone microscope was green when the emission filter was used, and it turned to blue immediately after removal of the emission filter (first and second rows in Figure S2). Through these experiments, we confirmed that the nonfluorescent particles in these mixtures (see the red arrows in Figure S2) do *not* appear in our cell phone images when the LP emission filter is used, clearly indicating that the detected signals on our cell phone images were indeed due to fluorescent emission, but not a result of scattering-related leakage of the excitation beam.

The brightness of 100 nm fluorescent particles that we imaged using our cell phone microscope was also characterized by a conventional confocal microscopy setup that is equipped with a hybrid photon-counting detector. To correlate the brightness of the fluorescence signal with the cluster size (*n*) of the fluorescent nanoparticles, the same sample of interest was imaged by our cell phone fluorescence microscope (Figure 3a), the photon-counting confocal microscope (Figure 3b), and an SEM (Figures 3c–i), sequentially. Cell phone fluorescence image depicts a heterogeneous distribution of fluorescence intensity which can be attributed to the formation of different sized nanoparticle clusters (Figure 3a). The photon-counting map shown in Figure 3b for the same sample illustrates a brightness distribution (expressed in photon counts per second, or cps) that matches very well to our cell-phone-based imaging results. The formation of nanoparticle clusters as well as the relationship between cluster size (*n*) and the brightness of signal was further validated by SEM;

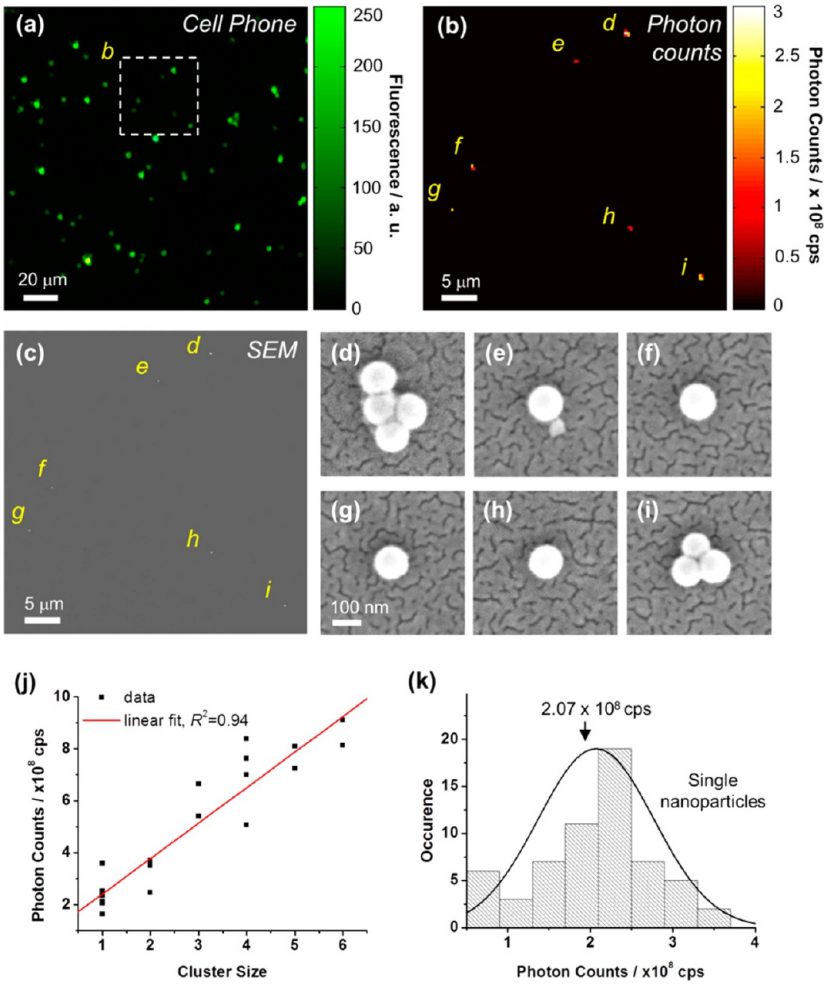

Figure 3. Brightness of 100 nm fluorescent particles characterized by photon counting. (a) Cell phone fluorescence image of 100 nm PS particles. (b) Photon-counting map that corresponds to the dashed area in (a), measured using a confocal laser scanning microscope. Note that the excitation conditions in (a) and (b) are different, which means the absolute photon count per second per particle might exhibit differences between the two images. (c) SEM image of the same area of photon-counting map shown in (b). (d−i) High-magnification SEM images of nanoparticle clusters highlighted in (c). (j) Correlation of the fluorescent photon counts per second per object as a function of the cluster size. (k) Fluorescent photon count distribution of single 100 nm particles (measured using 60 nanoparticles).

Figure 3c shows an SEM image of the same region as in Figure 3b and the dashed white square of Figure 3a. Higher-magnification SEM images (Figure 3d−i) reveal that four of these particles are single 100 nm particles ($n = 1$, Figure 3e−h), one is a tetramer ($n = 4$, Figure 3d), and one is a trimer ($n = 3$, Figure 3i). As expected, the nanoparticle clusters ($n \geq 2$, *e.g.*, Figure 3d,i) are brighter than the individual nanoparticles ($n = 1$, *e.g.*, Figure 3e−h) as also validated in both our cell phone fluorescence image (dashed region of Figure 3a) and the photon-counting map (Figure 3b). Quantitatively, the photon count per second for fluorescent nanoparticles is found to be linearly proportional to the size of the clusters with a fitting coefficient of 0.94 (see Figure 3j). For single 100 nm particles only, a brightness distribution is also shown in Figure 3k, revealing a mean fluorescent photon count of 2.07×10^8 cps. Previous studies have reported that a single fluorophore such as fluorescein or Alexa 488 exhibited a fluorescence emission rate on the order of 10^5 cps.[27−29] This suggests that there are approximately a few thousand fluorescein molecules embedded in a single 100 nm PS particle. However, note that the excitation and photon collection conditions in different experimental setups vary, which means the absolute photon count per second per particle might differ between different imaging systems.

In our cell phone microscopy platform, isolated 100 nm fluorescent particles can be readily detected over an area of 0.6 mm × 0.6 mm (Figure 2a), which, however, is smaller than the full FOV of our imaging platform (*i.e.*, ~3 mm × 3 mm). This relative reduction in our imaging FOV is due to the small spot size of our excitation laser beam (~1.8 mm in diameter) as well as the aberrations of the low NA imaging optics installed on our cell phone microscope. A measurement of the two-dimensional (2D) laser illumination profile on the sample plane shows that the excitation intensity drops rapidly at a distance that is larger than 0.3 mm away

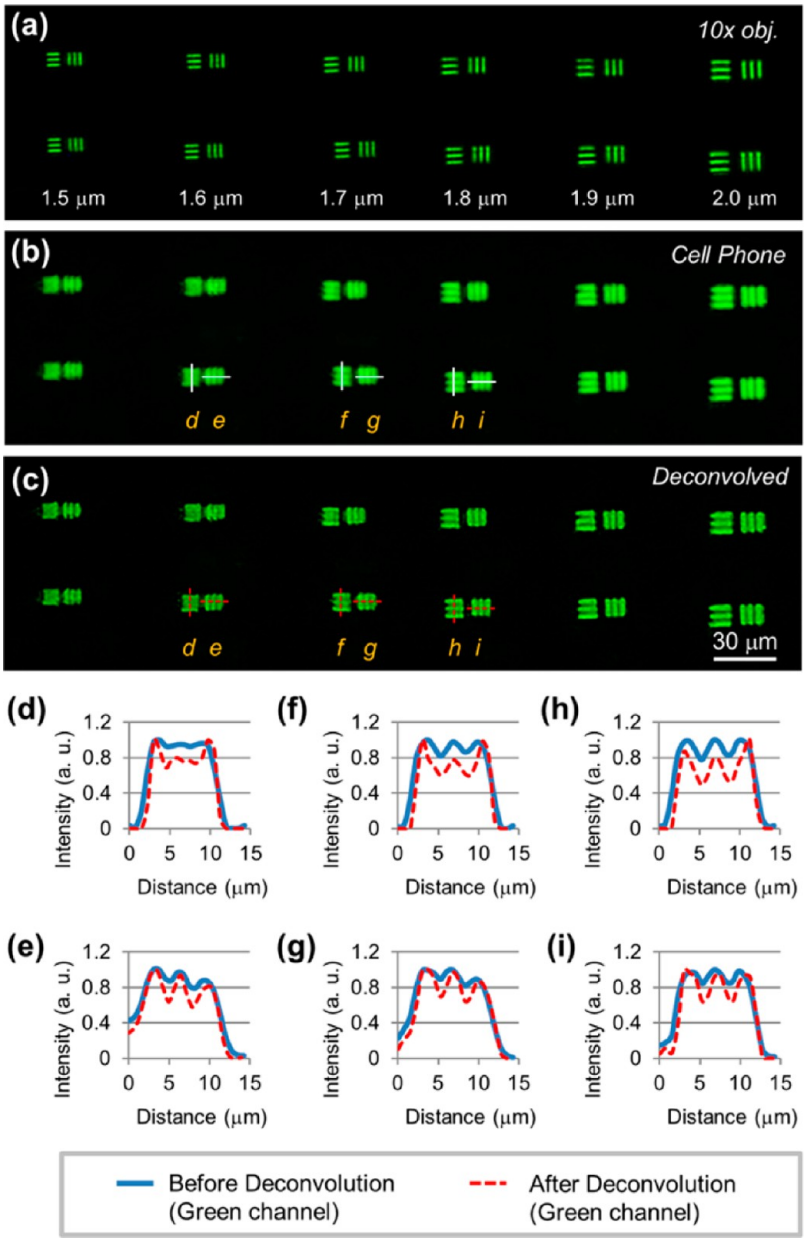

Figure 4. Spatial resolution test of the cell phone fluorescence microscope. (a) Transmission image of a resolution test target captured by a conventional microscope with a 10× objective lens (0.25 NA). (b) Same test target imaged by our cell phone microscope. (c) Deconvolved cell phone microscope image; isolated 100 nm fluorescent particles were used to estimate the point spread function of our microscope. (d–i) Line intensity profiles corresponding to the scanning lines in (b) and (c). Solid blue and dashed red lines are obtained from the green channel of the cell phone microscope image, before and after the Lucy–Richardson deconvolution, respectively.

from the center of the illumination area (Figure S1b). As a result of this, 100 nm fluorescent particles located outside of this 0.6 mm wide region are not excited efficiently. However, for larger sized objects which have stronger fluorescence emission and are less sensitive to imaging and focusing conditions, the object FOV can be significantly larger, reaching the entire 3 mm × 3 mm.

The spatial resolution of our cell phone fluorescence microscope was also characterized using a resolution test target fabricated by etching 200 nm thin gold–chromium (Au/Cr) film on a glass slide *via* e-beam lithography. This resolution target consists of various line patterns which have equal line widths and gap distances (ranging from 1.5 to 2.0 μm). Figure 4a,b shows the transmission images of this resolution test target acquired by a conventional microscope (10× objective lens, 0.25 NA) and our cell phone microscope, respectively. To mimic our fluorescence experiments, the illumination wavelength for these resolution tests was set to green (520 nm). Figure 4c depicts a deconvolved cell phone microscope image based on the Lucy–Richardson deconvolution algorithm[30,31] and a 2D point spread function (PSF) that is estimated using

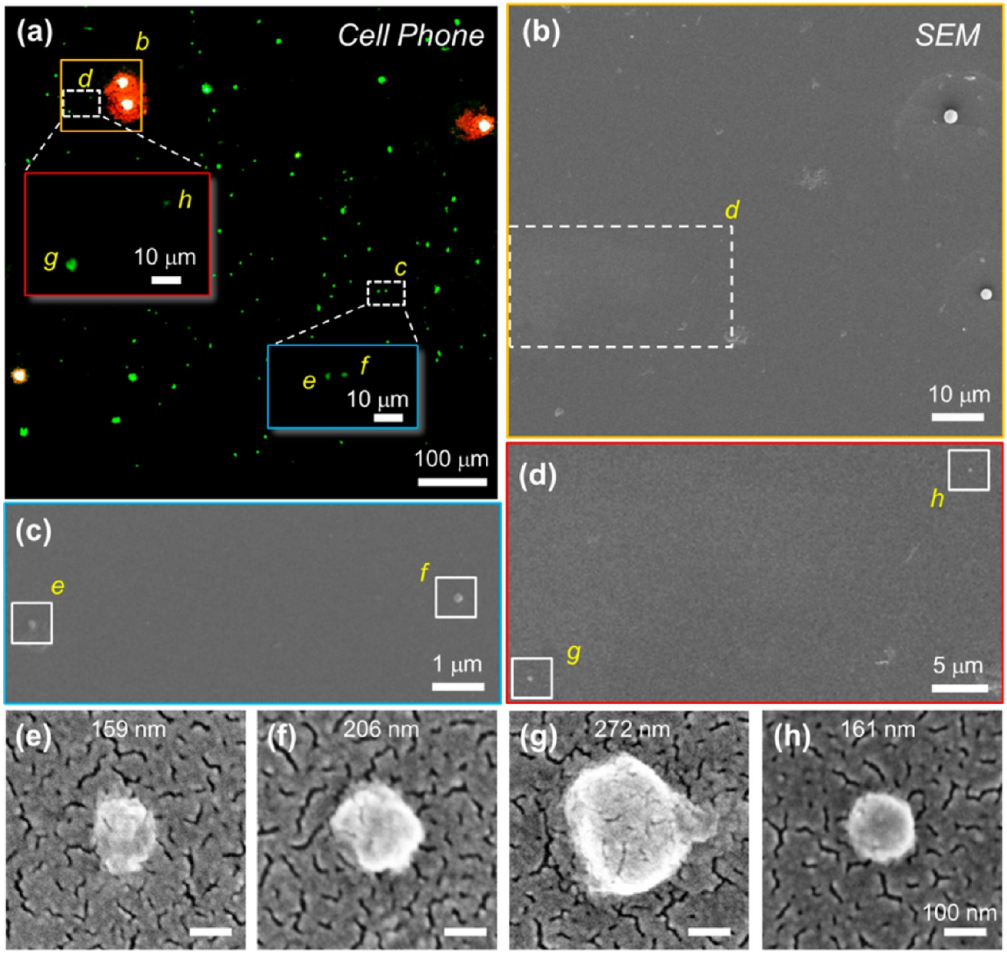

Figure 5. Single-virus imaging on the cell phone. (a) Cell phone fluorescence image of Alexa-488-labeled HCMV particles; 2 μm red fluorescent beads were used as location markers for SEM comparison images. (b,c) SEM images of the regions corresponding to the dashed boxes in (a). (d) Enlarged view of the boxed area in (b). (e−h) High-magnification SEM images of individual HCMV particles highlighted by the solid boxes in (c) and (d). The same isolated viral particles are also highlighted within the inset fluorescence images of (a).

isolated 100 nm fluorescent particles. Line intensity profiles of 1.6, 1.7, and 1.8 μm bars before (solid blue curves) and after deconvolution (dashed red curves) are shown in Figure 4d−i. Even before Lucy−Richardson deconvolution is applied, our cell phone microscope was able to resolve 1.7 μm bars along both the horizontal and vertical directions, as well as 1.5 μm bars along the horizontal direction (Figure 4d−g). After deconvolution, 1.6 μm bars along the vertical direction (Figure 4d) and 1.5 μm bars along the horizontal direction were better resolved.

Single-Virus Imaging Experiments. To further demonstrate the imaging performance of our cell-phone-based fluorescent microscope, we also imaged individual HCMV particles. HCMV is a member of the herpes virus family that causes severe mortality especially in immunocompromised patients.[10] It is also one of the leading causes of virus-associated birth defects, such as mental retardation and deafness.[10] HCMV virus particle consists of genome, capsid, tegument, and a lipid bilayer envelope with an overall particle size ranging from 150 to 300 nm in diameter.[32] To label intact HCMV particles, we first targeted glycoprotein B (gB) molecule, which is one of the most abundant glycoproteins on the virus envelope[33] with anti-gB primary antibody, and then labeled the virions with Alexa-488-conjugated secondary antibody (refer to the Methods section for further details). Conventional fluorescence microscopy confirmed the successful fluorescent labeling of HCMVs on glass slides (see Figure S3b,d), whereas our control samples containing only primary and secondary antibodies did not show significant fluorescent backgrounds (Figure S3a,c). For cell-phone-based detection of single viruses, fluorescence images of labeled HCMV samples were acquired under similar imaging conditions as fluorescent nanoparticles. A representative cell phone fluorescent image of labeled HCMV particles is shown in Figure 5a, where red fluorescent PS beads (2 μm in diameter) were added to provide location markers for SEM comparison, as also detailed in our Methods section. Two different ROIs containing isolated viral particles are highlighted with the dashed white

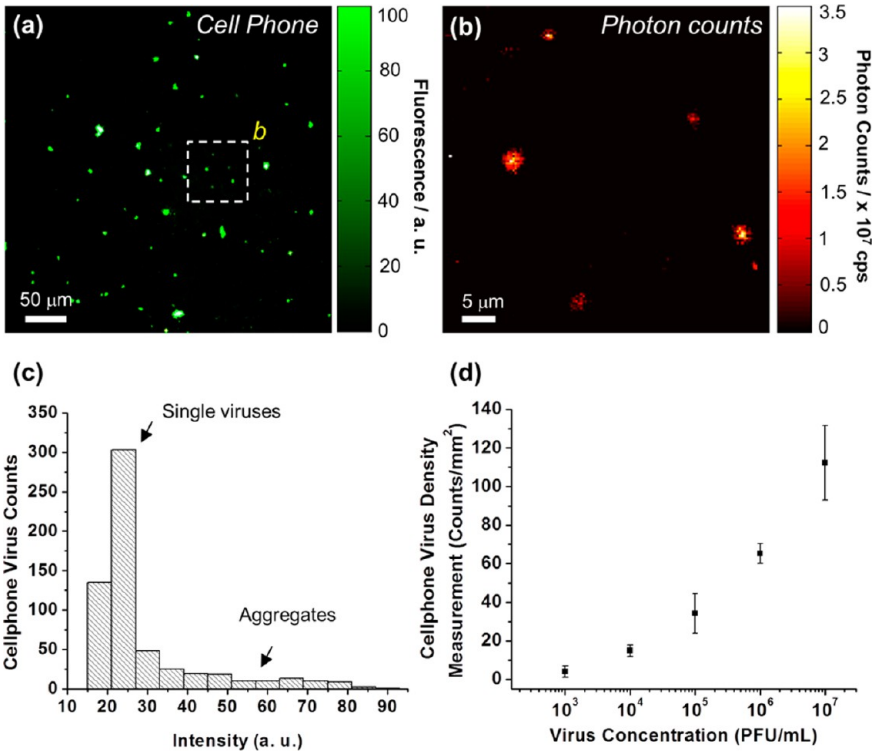

Figure 6. Fluorescent signal intensity comparison for HCMV particles. (a) Cell phone fluorescence image of labeled HCMV particles at an incubation concentration of 10^7 PFU/mL. (b) Photon-counting map corresponding to the dashed area in (a), measured using a confocal laser scanning microscope. Note that the excitation conditions in (a) and (b) are different, which means the absolute photon count per second per particle might exhibit differences between the two images. (c) Distribution of the intensity of the labeled HCMV particles in the cell phone fluorescent images. (d) Cell-phone-based virus density measurements (counts/mm^2) plotted against different virus incubation concentrations (10^3, 10^4, 10^5, 10^6, and 10^7 PFU/mL). Three independent measurements for each concentration were performed.

boxes as well as the insets in Figure 5a, and their corresponding SEM images are also shown in Figure 5b,c, respectively. Figure 5d is an enlarged SEM image taken from the dashed area in Figure 5b. The green fluorescent dots highlighted by the dashed boxes and the insets in Figure 5a were thus confirmed by the high-magnification SEM images to be single virus particles, as shown in Figure 5e−h. According to our SEM measurements, the size of each HCMV particle varied between 159 and 272 nm, which provides a decent match to the previous reports on HCMV.[32]

The detection of single fluorescently labeled virus particles is challenging due to the low fluorophore labeling density per virus particle. Our photon-counting analysis suggests that the brightness of labeled HCMV particles is approximately an order of magnitude weaker (10^7 cps, Figure 6b) than that of individual 100 nm fluorescent particles (10^8 cps, Figure 3b). This implies that a labeling density on the order of a few hundred fluorophores per virus particle was achieved through our surface marker labeling strategy. The fluorescence signal of labeled virus particles detected using our cell phone microscope also displayed a broad distribution as revealed by single-particle analysis shown in Figure 6c. The major peak at the low-intensity region (a.u. < ~30) can be attributed to isolated virus particles, whereas the distribution with higher fluorescent intensities is due to virus aggregates (Figure 6c). We also measured the density of virus particles (counts/mm^2) using our cell phone images which, as desired, exhibited a strong dependence on the initial incubation concentration (PFU/mL) of virus solutions (Figure 6d). Our control sample (without any virus particles but only treated with primary and secondary antibodies) displayed an averaged fluorescent spot density of 12.7 ± 0.8 counts/mm^2. After subtracting this background value, our samples incubated with 10^3, 10^4, 10^5, 10^6, and 10^7 PFU/mL of HCMV particles yielded cell-phone-based viral density measurements of 3.9 ± 2.9, 14.9 ± 3.0, 34.2 ± 10.2, 65.2 ± 5.2, and 112.3 ± 19.2 counts/mm^2, respectively (Figure 6d), which demonstrates the correlation between our cell-phone-based virus density measurements (*i.e.*, counts/mm^2) and the initial incubation concentration of the viral load (*i.e.*, PFU/mL).

These imaging results constitute the first time that a cell-phone-based field-portable microscopy platform has detected isolated/individual viruses and nanoscale fluorescent objects. This new imaging performance presented in our work should provide a complementary addition to other cell-phone-based microscopy, sensing, and diagnostics tools, enabling various new

nanotechnology applications for especially telemedicine and point-of-care testing/analysis.

CONCLUSIONS

We demonstrated a field-portable fluorescence microscopy platform installed on a smart phone for imaging of single nanoparticles and viruses. The design of this hand-held fluorescence imaging device installed on the cell phone includes a 450 nm laser diode, a LP thin-film interference filter, a low NA external lens, and a translation stage for focusing. Our imaging device overcomes SNR limitations by utilizing (i) a high-power excitation source to enhance the fluorescence emission, (ii) a high illumination angle, and (iii) a thin-film interference filter to reduce/suppress the background noise. We tested the performance of our cell phone microscope by detecting individual 100 nm fluorescent particles as well as single HCMVs that are fluorescently labeled. Given its high sensitivity and field-portability, our cell-phone-based fluorescence imaging platform could be useful for specific imaging of various fluorescently labeled specimen such as bacteria and viruses in field settings. Therefore, it holds significant promise for various point-of-care applications such as viral load measurements or other biomedical tests conducted in remote or resource-limited environments.

METHODS

Opto-Mechanical Design of the Cell Phone Microscope Attachment. The three-dimensional (3D) opto-mechanical attachment to our cell phone (PureView 808, Nokia) was designed using Inventor software (Autodesk) and built by a 3D printer (Elite, Dimension). A compact blue laser diode (eBay) that was mounted on a 12 × 30 mm copper module (also used as a *heat-sink*) was used as the excitation light source and powered by three AAA batteries. The laser diode provides a narrow-band excitation centered at 450 nm (fwhm = 2 nm) with a total output power of ~75 mW. The spectrum and optical power of this laser diode were measured by a HR2000+ spectrometer (Ocean Optics) and PM100 optical power meter (Thorlabs), respectively. The sample slide of interest was illuminated by this blue laser diode with a 75° incidence angle, and its position was controlled using a miniature dovetail stage (DT12, Thorlabs) for focus adjustment. The fluorescence emission from the specimen was collected by an external lens (f_1 = 4 mm) and was separated from the excitation light by using a 2 mm thick 500 nm long-pass thin-film interference filter (FF01-500/LP-23.3-D, Semrock) that was positioned after the sample (see Figure 1d). Magnified fluorescent images of the specimen were formed using both the external lens and the built-in lens (f_2 = 8 mm) of the cell phone camera and were recorded by the CMOS sensor chip (7728 × 5386 pixels, pixel size = 1.4 μm) embedded on the cell phone.

Preparation of the Fluorescent Particle Samples. Green fluorescent polystyrene (PS) particles (excitation/emission: 505/515 nm) with various sizes (0.1, 0.25, 0.5, 1, 2, 4, and 10 μm) were obtained from Invitrogen. For imaging isolated particles, the samples were diluted 10^4–10^5 times in deionized (DI) water. Glass coverslips (18 × 18 mm, No. 1, Thermo Fisher) were rinsed sequentially with acetone, isopropyl alcohol, methanol, and DI water and dried by nitrogen blow. Cleaned coverslips were further treated by plasma (BD-10AS, Electro-Technic Products, Inc.) for a duration of 5–10 s to hydrophilize the surface. Finally, 2 μL of diluted solution was pipetted onto the treated glass coverslips and dried at room temperature (RT) before imaging.

Fluorescent Labeling of Human Cytomegaloviruses (HCMVs). For immobilization of HCMV particles, glass coverslips (9 × 9 mm, No. 1, Electron Microscopy Sciences) were washed and dried as previously described. The surface of each glass substrate was functionalized with amino groups by immersion in 2% (v/v) solution of 3-aminopropyltriethoxysilane (Sigma) in acetone for 10 min at RT. Coated slides were rinsed thoroughly with acetone and DI water and allowed to dry in nitrogen blow. Then, 250 μL of cell-culture supernatant containing HCMV viruses at various concentrations ranging from 10^3 to 10^7 plaque forming units per mL (PFU/mL) was seeded onto each amine-functionalized glass slide in a 24-well plate overnight. The culture medium was then removed, and the virus particles were fixed and immobilized onto glass substrates by treating with cross-linking buffer containing 2% paraformaldehyde (Sigma) and 0.1% glutaraldehyde (Sigma) in phosphate buffered saline (PBS) for 2 h. Excess cross-linkers were quenched by Tris buffered saline (TBS, 500 mM Tris) for 30 min. These substrates were then blocked from nonspecific protein–protein interactions using the blocking buffer containing 3% bovine serum albumin (BSA), 10% fetal bovine serum (FBS), and 0.1% TritonX-100 in TBS for 1 h. The glass slides that contained immobilized viral particles were then washed with TBS (50 mM Tris) three times and followed by incubation with mouse monoclonal antibody (CH446, Virusys Corp) against HCMV glycoprotein B at 10 μg/mL for 1 h. Unbound antibodies were removed by washing three times with TBS (50 mM Tris). The sample slides were further incubated with 2 μg/mL of Alexa-488-conjugated secondary antibody against mouse IgG for 1 h and washed three times with TBS (50 mM Tris). Finally, the labeled virus slides were dried by nitrogen blow. On each slide, to provide location markers, we also added 2 μm diameter red fluorescent PS particles (excitation/emission: 580/605 nm; from Invitrogen) which helped us to better define regions of interest and search for the specific locations that contain isolated viral particles within our large field of view so that we can compare our cell-phone-based fluorescent imaging results against SEM images.

Photon-Counting Microscopy. The brightness of 100 nm fluorescent particles and Alexa-488-labeled HCMV virus particles was independently characterized by using a confocal laser scanning microscope (TCS SP8, Leica) equipped with a high NA objective (HCX PL APO CS 63×/1.40 oil) and a hybrid detector (HyD, Leica) that is capable of recording photon streams. Photon-counting maps (512 × 512 pixels) were collected using 488 nm laser excitation and a 510–560 nm band-pass emission filter. The laser beam was scanned at a rate of 1.2 μs/pixel with 8 accumulated scanning per line, resulting in an effective pixel dwell time of 9.6 μs/pixel.

SEM Comparison Experiments. An FEI Nova 600 instrument operating at 10 kV was used to validate the size of individual nanoparticles or viruses imaged on our cell-phone-based fluorescent microscope. After imaging with the cell phone microscope, all the sample slides were sputtered with gold conductive layer for 60 s before SEM imaging experiments were performed.

Conflict of Interest: The authors declare the following competing financial interest(s): A. Ozcan is the co-founder of a start-up company (Holomic LLC) that aims to commercialize computational microscopy and sensing tools.

Acknowledgment. Ozcan Research Group gratefully acknowledges the support of Nokia University Cooperation Funding, the Presidential Early Career Award for Scientists and Engineers (PECASE), Army Research Office (ARO) Life Sciences Division, ARO Young Investigator Award, National Science Foundation (NSF) CAREER Award, NSF CBET Division Biophotonics Program, NSF Emerging Frontiers in Research and Innovation (EFRI) Award, Office of Naval Research (ONR) Young Investigator Award and National Institutes of Health (NIH)

Director's New Innovator Award DP2OD006427 from the Office of the Director, National Institutes of Health. The authors also acknowledge Xinghong Dai in Hong Zhou's Lab (Department of Microbiology, Immunology, and Molecular Genetics, UCLA) and Danyang Gong in Ren Sun's Lab for providing the HCMV samples. Photon-counting microscopy experiments were performed at the California NanoSystems Institute Advanced Light Microscopy/Spectroscopy Imaging Facility at UCLA.

Supporting Information Available: Spectrum of long-pass filter, spectrum and 2D intensity profile of laser diode, cell-phone-based fluorescence images of different sized PS beads and experimental validation of fluorescent staining/labeling of HCMVs. This material is available free of charge *via* the Internet at http://pubs.acs.org.

REFERENCES AND NOTES

1. Van Dijk, M. A.; Lippitz, M.; Orrit, M. Far-Field Optical Microscopy of Single Metal Nanoparticles. *Acc. Chem. Res.* **2005**, *38*, 594–601.
2. Yurt, A.; Daaboul, G. G.; Connor, J. H.; Goldberg, B. B.; Unlü, S. M. Single Nanoparticle Detectors for Biological Applications. *Nanoscale* **2012**, *4*, 715–726.
3. Boyer, D.; Tamarat, P.; Maali, A.; Lounis, B.; Orrit, M. Photothermal Imaging of Nanometer-Sized Metal Particles among Scatterers. *Science* **2002**, *297*, 1160–1163.
4. Lindfors, K.; Kalkbrenner, T.; Stoller, P.; Sandoghdar, V. Detection and Spectroscopy of Gold Nanoparticles Using Supercontinuum White Light Confocal Microscopy. *Phys. Rev. Lett.* **2004**, *93*, 037401.
5. Hong, X.; van Dijk, E. M. P. H.; Hall, S. R.; Götte, J. B.; van Hulst, N. F.; Gersen, H. Background-Free Detection of Single 5 nm Nanoparticles through Interferometric Cross-Polarization Microscopy. *Nano Lett.* **2011**, *11*, 541–547.
6. Bu, X.; Chen, H.; Gai, H.; Yang, R.; Yeung, E. S. Scattering Imaging of Single Quantum Dots with Dark-Field Microscopy. *Anal. Chem.* **2009**, *81*, 7507–7509.
7. Hu, M.; Novo, C.; Funston, A.; Wang, H.; Staleva, H.; Zou, S.; Mulvaney, P.; Xia, Y.; Hartland, G. V. Dark-Field Microscopy Studies of Single Metal Nanoparticles: Understanding the Factors That Influence the Linewidth of the Localized Surface Plasmon Resonance. *J. Mater. Chem.* **2008**, *18*, 1949–1960.
8. Daaboul, G. G.; Yurt, A.; Zhang, X.; Hwang, G. M.; Goldberg, B. B.; Unlü, M. S. High-Throughput Detection and Sizing of Individual Low-Index Nanoparticles and Viruses for Pathogen Identification. *Nano Lett.* **2010**, *10*, 4727–4731.
9. Mudanyali, O.; McLeod, E.; Luo, W.; Greenbaum, A.; Coskun, A. F.; Hennequin, Y.; Allier, C. P.; Ozcan, A. Wide-Field Optical Detection of Nanoparticles Using On-Chip Microscopy and Self-Assembled Nanolenses. *Nat. Photonics* **2013**, *7*, 240–247.
10. Huang, E.-S.; Johnson, R. A. Human Cytomegalovirus—No Longer Just a DNA Virus. *Nat. Med.* **2000**, *6*, 863–864.
11. Tseng, D.; Mudanyali, O.; Oztoprak, C.; Isikman, S. O.; Sencan, I.; Yaglidere, O.; Ozcan, A. Lensfree Microscopy on a Cellphone. *Lab Chip* **2010**, *10*, 1787–1792.
12. Mudanyali, O.; Tseng, D.; Oh, C.; Isikman, S. O.; Sencan, I.; Bishara, W.; Oztoprak, C.; Seo, S.; Khademhosseini, B.; Ozcan, A. Compact, Light-Weight and Cost-Effective Microscope Based on Lensless Incoherent Holography for Telemedicine Applications. *Lab Chip* **2010**, *10*, 1417–1428.
13. Zhu, H.; Yaglidere, O.; Su, T.-W.; Tseng, D.; Ozcan, A. Cost-Effective and Compact Wide-Field Fluorescent Imaging on a Cell-Phone. *Lab Chip* **2011**, *11*, 315–322.
14. Zhu, H.; Mavandadi, S.; Coskun, A. F.; Yaglidere, O.; Ozcan, A. Optofluidic Fluorescent Imaging Cytometry on a Cell Phone. *Anal. Chem.* **2011**, *83*, 6641–6647.
15. Zhu, H.; Sikora, U.; Ozcan, A. Quantum Dot Enabled Detection of *Escherichia coli* Using a Cell-Phone. *Analyst* **2012**, *137*, 2541–2544.
16. Mudanyali, O.; Dimitrov, S.; Sikora, U.; Padmanabhan, S.; Navruz, I.; Ozcan, A. Integrated Rapid-Diagnostic-Test Reader Platform on a Cellphone. *Lab Chip* **2012**, *12*, 2678–2686.
17. Zhu, H.; Sencan, I.; Wong, J.; Dimitrov, S.; Tseng, D.; Nagashima, K.; Ozcan, A. Cost-Effective and Rapid Blood Analysis on a Cell-Phone. *Lab Chip* **2013**, *13*, 1282–1288.
18. Coskun, A. F.; Wong, J.; Khodadadi, D.; Nagi, R.; Tey, A.; Ozcan, A. A Personalized Food Allergen Testing Platform on a Cellphone. *Lab Chip* **2013**, *13*, 636–640.
19. Greenbaum, A.; Luo, W.; Su, T.-W.; Gorocs, Z.; Xue, L.; Isikman, S. O.; Coskun, A. F.; Mudanyali, O.; Ozcan, A. Imaging without Lenses: Achievements and Remaining Challenges of Wide-Field on-Chip Microscopy. *Nat. Methods* **2012**, *9*, 889–895.
20. Granot, Y.; Ivorra, A.; Rubinsky, B. A New Concept for Medical Imaging Centered on Cellular Phone Technology. *PLoS One* **2008**, *3*, e2075.
21. Breslauer, D. N.; Maamari, R. N.; Switz, N. A.; Lam, W. A.; Fletcher, D. A. Mobile Phone Based Clinical Microscopy for Global Health Applications. *PLoS One* **2009**, *4*, e6320.
22. Smith, Z. J.; Chu, K.; Espenson, A. R.; Rahimzadeh, M.; Gryshuk, A.; Molinaro, M.; Dwyre, D. M.; Lane, S.; Matthews, D.; Wachsmann-Hogiu, S. Cell-Phone-Based Platform for Biomedical Device Development and Education Applications. *PLoS One* **2011**, *6*, e17150.
23. Gallegos, D.; Long, K. D.; Yu, H.; Clark, P. P.; Lin, Y.; George, S.; Nath, P.; Cunningham, B. T. Label-Free Biodetection Using a Smartphone. *Lab Chip* **2013**, *13*, 2124–2132.
24. Oncescu, V.; O'Dell, D.; Erickson, D. Smartphone Based Health Accessory for Colorimetric Detection of Biomarkers in Sweat and Saliva. *Lab Chip* **2013**, *13*, 3232–3238.
25. Shen, L.; Hagen, J. A.; Papautsky, I. Point-of-Care Colorimetric Detection with a Smartphone. *Lab Chip* **2012**, *12*, 4240–4243.
26. You, D. J.; Park, T. S.; Yoon, J.-Y. Cell-Phone-Based Measurement of TSH Using Mie Scatter Optimized Lateral Flow Assays. *Biosens. Bioelectron.* **2013**, *40*, 180–185.
27. Chen, Y.; Müller, J. D.; So, P. T. C.; Gratton, E. The Photon Counting Histogram in Fluorescence Fluctuation Spectroscopy. *Biophys. J.* **1999**, *77*, 553–567.
28. Hillesheim, L. N.; Müller, J. D. The Photon Counting Histogram in Fluorescence Fluctuation Spectroscopy with Non-ideal Photodetectors. *Biophys. J.* **2003**, *85*, 1948–1958.
29. Mukhopadhyay, S.; Krishnan, R.; Lemke, E. A.; Lindquist, S.; Deniz, A. A. A Natively Unfolded Yeast Prion Monomer Adopts an Ensemble of Collapsed and Rapidly Fluctuating Structures. *Proc. Natl. Acad. Sci. U.S.A.* **2007**, *104*, 2649–2654.
30. Richardson, W. H. Bayesian-Based Iterative Method of Image Restoration. *J. Opt. Soc. Am.* **1972**, *62*, 55–59.
31. Lucy, L. B. An Iterative Technique for the Rectification of Observed Distributions. *Astron. J.* **1974**, *79*, 745–754.
32. Haspot, F.; Lavault, A.; Sinzger, C.; Laib Sampaio, K.; Stierhof, Y.-D.; Pilet, P.; Bressolette-Bodin, C.; Halary, F. Human Cytomegalovirus Entry into Dendritic Cells Occurs *via* a Macropinocytosis-like Pathway in a pH-Independent and Cholesterol-Dependent Manner. *PLoS One* **2012**, *7*, e34795.
33. Varnum, S. M.; Streblow, D. N.; Monroe, M. E.; Smith, P.; Auberry, K. J.; Paša-Tolić, L.; Wang, D.; Camp, D. G.; Rodland, K.; Wiley, S.; *et al.* Identification of Proteins in Human Cytomegalovirus (HCMV) Particles: The HCMV Proteome. *J. Virol.* **2004**, *78*, 10960–10966.